Class. Quantum Grav. **24** (2007) S433–S443 doi:10.1088/0264-9381/24/19/S07

Analysis of noise lines in the Virgo C7 data

F Acernese[1], P Amico[2], M Alshourbagy[3], F Antonucci[4], S Aoudia[5], P Astone[4], S Avino[1], D Babusci[6], G Ballardin[7], F Barone[1], L Barsotti[3], M Barsuglia[8], Th S Bauer[9], F Beauville[10], S Bigotta[3], S Birindelli[3], M A Bizouard[8], C Boccara[11], F Bondu[5], L Bosi[2], C Bradaschia[3], S Braccini[3], F J van den Brand[9], A Brillet[5], V Brisson[8], D Buskulic[10], E Calloni[1], E Campagna[12], F Carbognani[7], F Cavalier[8], R Cavalieri[7], G Cella[3], E Cesarini[12], E Chassande-Mottin[5], N Christensen[7], C Corda[3], A Corsi[4], F Cottone[2], A-C Clapson[8], F Cleva[5], J-P Coulon[5], E Cuoco[7], A Dari[2], V Dattilo[7], M Davier[8], M del Prete[3], R De Rosa[1], L Di Fiore[1], A Di Virgilio[3], B Dujardin[5], A Eleuteri[1], M Evans[7], I Ferrante[3], F Fidecaro[3], I Fiori[7], R Flaminio[7,10], J-D Fournier[5], S Frasca[4], F Frasconi[3], L Gammaitoni[2], F Garufi[1], E Genin[7], A Gennai[3], A Giazotto[3], G Giordano[6], L Giordano[1], R Gouaty[10], D Grosjean[10], G Guidi[12], S Hamdani[7], S Hebri[7], H Heitmann[5], P Hello[8], D Huet[7], S Karkar[10], S Kreckelbergh[8], P La Penna[7], M Laval[5], N Leroy[8], N Letendre[10], B Lopez[7], Lorenzini[12], V Loriette[11], G Losurdo[12], J-M Mackowski[13], E Majorana[4], C N Man[5], M Mantovani[3], F Marchesoni[2], F Marion[10], J Marque[7], F Martelli[12], A Masserot[10], M Mazzoni[12], L Milano[1], F Menzinger[7], C Moins[7], J Moreau[11], N Morgado[13], B Mours[10], F Nocera[7], C Palomba[4], F Paoletti[3,7], S Pardi[1], A Pasqualetti[7], R Passaquieti[3], D Passuello[3], F Piergiovanni[12], L Pinard[13], R Poggiani[3], M Punturo[2], P Puppo[4], S van der Putten[9], K Qipiani[1], P Rapagnani[4], V Reita[11], A Remillieux[13], F Ricci[4], I Ricciardi[1], P Ruggi[7], G Russo[1], S Solimeno[1], A Spallicci[5], M Tarallo[3], M Tonelli[3], A Toncelli[3], E Tournefier[10], F Travasso[2], C Tremola[3], G Vajente[3], D Verkindt[10], F Vetrano[12], A Viceré[12], J-Y Vinet[5], H Vocca[2] and M Yvert[10]

[1] INFN, Sezione di Napoli and/or Università di Napoli 'Federico II' Complesso Universitario di Monte S Angelo, and/or Università di Salerno, Fisciano (Sa), Italy
[2] INFN, Sezione di Perugia and/or Università di Perugia, Perugia, Italy
[3] INFN, Sezione di Pisa and/or Università di Pisa, Pisa, Italy
[4] INFN, Sezione di Roma and/or Università 'La Sapienza', Roma, Italy
[5] Departement Artemis—Observatoire de la Côte d'Azur, BP 42209 06304 Nice, Cedex 4, France
[6] INFN, Laboratori Nazionali di Frascati, Frascati (Rm), Italy
[7] European Gravitational Observatory (EGO), Cascina (Pi), Italy
[8] LAL, Univ Paris-Sud, IN2P3/CNRS, Orsay, France
[9] NIKHEF, NL-1009 DB Amsterdam and/or Vrije Universiteit, NL-1081 HV Amsterdam, The Netherlands
[10] Laboratoire d'Annecy-le-Vieux de Physique des Particules (LAPP), IN2P3/CNRS, Université de Savoie, Annecy-le-Vieux, France
[11] ESPCI, Paris, France
[12] INFN, Sezione di Firenze/Urbino, Sesto Fiorentino, and/or Università di Firenze, and/or Università di Urbino, Italy
[13] LMA, Villeurbanne, Lyon, France

E-mail: nelson.christensen@ego-gw.it and irene.fiori@ego-gw.it

0264-9381/07/190433+11$30.00

Received 18 April 2007, in final form 4 June 2007
Published 19 September 2007
Online at stacks.iop.org/CQG/24/S433

Abstract
The paper presents a description of the work of detection and identification of frequency lines in the Virgo dark fringe data from run C7. A number of methods are highlighted by which noise frequency lines are detected by data analysis and measurements in the laboratory. In this paper we give a description of the list of noise line candidates provided by the pulsar search analysis, the investigation of 10 Hz (and harmonics) noise, violin modes, noise from the end station buildings' air conditioners, sidebands in calibration lines and aliasing in the 4 kHz reconstructed data.

PACS numbers: 04.80.Nn, 07.05.Kf, 95.55.Ym

(Some figures in this article are in colour only in the electronic version)

1. Introduction

The scientific goal of the Virgo interferometer is the detection of gravitational wave signals in the 10 Hz to 10 kHz frequency band [1]. Virgo is in the final commissioning phase, and one major activity is the hunting of control and environmental noise. Persistent frequency peaks (lines) in the interferometer output signal can originate, for example, from standard interferometer functions and operations (mirror resonance, calibration lines, etc), from environmental perturbations (i.e. electro-mechanical devices), and from non-stationary noise (i.e. sideband structures). This paper presents a description of the work on the detection and investigation of the origin of the noise frequency lines in the Virgo dark fringe data from run C7.

The C7 run took place from 14 September through 19 September 2005; the duty cycle for this run was 65%. A number of data analysis techniques and experimental methods (in the laboratory) were used to identify and characterize noise lines. A first list of lines were generated using the search algorithm used by the on-line monitor and described in [2] and section 2. Line candidates also come as the by-product of the analysis pipeline of the periodic signal search (PSS) performed by the Virgo pulsar search group. We discuss this new line catalogue in section 3 and compare the results with the outcome of the other search method. We also used a newly implemented catalogue of environmental coherences [3] and a multi-coherence tool [4] to investigate the origin of environmental lines. We searched for a match between our line candidates and large coherence values with environmental channels; this is described in section 5. Then a *hunt* was conducted for the sources of these lines by surveying the experimental halls with portable measurement equipment (accelerometers, Hall probes and microphones). We identified some lines as originating from the air conditioning in the end stations; we also found the source of a 10 Hz noise line source, see section 6. Other lines that were identified include: mirror modes and violin modes of mirror wires (see section 7, which includes a measurement of the ring-down decay time of these lines), sidebands of calibration lines (section 4), and lines due to the residual aliasing in the 4 kHz down-sampled data (section 8). For better or worse, our investigation only identifies noise lines of constant

frequency; wandering lines are another type of problem, but they are not addressed in this paper.

2. Lines from the on-line algorithm

An initial list of line candidates was produced by the on-line monitor of the Virgo dark fringe photodiode signal. The monitor uses the line search algorithm described in [2], and the choice of the parameter values was made in order to optimize its operation as an on-line application. Briefly, the algorithm proceeds in three steps.

(i) The signal's average amplitude spectrum is computed over time windows of length T_w with spectral resolution $\sigma_f = 1/T$ ($T_w \simeq 240$ s and $T \simeq 13$ s were used).
(ii) The frequency axis is tiled in intervals of minimum size N_n ($N_n = 64$ was used) increasing in a dyadic way, with $N_i = 2^i N_n N_b$ being the size of the ith interval ($N_b = 8$ is used). In each interval the algorithm computes a linear fit of the data points, excluding the N_q points with the largest amplitude ($N_q = 32$ was used); this fit estimates the background spectral noise.
(iii) Within each interval the algorithm selects the frequency points whose amplitude exceeds the background by more than the SNR threshold (SNR $= 5$ is used).

The output of the algorithm over the entire C7 science mode dataset (about 100 h) consisted of 61 516 frequency peaks, occupying 824 different frequency bins. From this map of time–frequency data points we extracted a list of 70 lines by performing the post-processing steps.

(i) Select and list separately the harmonics of the 50 Hz power line (the nth harmonic is identified as the group of points within the frequency window of width $n \times \sigma_f$ around the frequency value $n \times 50$ Hz); 19 lines were identified as 50 Hz harmonics.
(ii) Select 'persistent' frequencies[14] [14], existing for at least 3% of total time: 155 frequencies were selected.
(iii) Merge frequencies in consecutive frequency bins, then assign to the candidate line the average frequency value and a line width equal to σ_f times the number of merged bins; 70 lines were detected at this step.

Note that wandering lines might exist whose frequency changes with time, for example, driven by temperature changes. The time–frequency map shows that there are few lines in C7 which have a large drift. These are either missed or averaged out by out post-processing cuts. In section 3, we describe a second method we used to derive a list of lines in the C7 dark fringe signal.

3. Lines from the pulsars search

A list of persistent and high-resolution frequency peaks comes as a by-product of a preliminary step in the analysis pipeline that searches for periodic gravitational wave (GW) signals from pulsars. The pulsar search group set up an analysis procedure to search for periodic signals in the Virgo strain sensitivity channel. As described in [5], the PSS analysis pipeline first performs a data cleaning, identifying and removing transient time domain disturbances. Then

[14] Frequency peaks with low persistence are likely associated with (i) random spectral fluctuations of the noise or (ii) noise bursts or (iii) mistakes of the search algorithm, typically occurring in the presence of broad peaks or not flat spectral backgrounds. The number of these fake frequency peaks scales with the fraction of total runtime. The chosen cut eliminates about 9% of the frequency peaks and about 80% of the occupied frequency bins.

it produces collections of FFTs of various lengths over the entire science mode dataset. The subsequent step is an adaptive search for frequency peaks in these spectra. An auto-regressive average spectrum is computed which gives a good estimate of the spectral background noise; then the ratio is taken of the FFT to the average spectrum and the data that exceed a given threshold SNR are selected. At this step, the PSS analysis outputs a list of frequency peaks and a record of the number of FFT containing that peak, i.e. the fraction of the total observation time the peak exists. This is our list of candidate lines.

The list of lines derived in this way has some advantages with respect to those found via the method described in section 2: (i) it profits from the data cleaning performed by the PSS analysis; (ii) the PSS produces datasets of frequency peaks from higher resolution FFTs (up to 16 000 s) that could be used if a more comprehensive list of lines is desired; (iii) being that it is a by-product of the pulsar search analysis it will come with no additional computational costs. The pulsar search algorithm is preferred for the purpose of providing a high-resolution list of noise lines, whereas the search algorithm described in section 2 yields rapid information and quick access to results.

For C7 the PSS analysis pipeline, still in a test phase, was run on the strain reconstructed channel down-sampled to 4 kHz and with an FFT resolution of $T \simeq 100$ s over the frequency range 0–2000 Hz. The output consisted of about 280 000 frequency peaks, out of which 676 had a persistence longer than 3% of the C7 science dataset. The 3% persistence threshold is admittedly somewhat arbitrary, but it provided a reasonable number of candidate lines that could then be realistically studied by our research team. This number was then reduced to 376 after the merging step described in section 2 and after removing the power line harmonics.

This lines dataset includes the results from the search algorithm for frequencies below 2 kHz. Among the ∼400 candidate noise lines from the two lists, some (18 lines) are known from previous investigations, such as those from the vacuum pumps [6] and mirror thermal modes [7], while some are calibration lines (7 lines). Sections 4–8 describe the work of identifying the origin of the remaining unknown lines. These lines belong to seven categories: oscillation modes of the super attenuator (13 lines, section 4), sidebands of calibration lines (41 lines, section 4), lines from environmental perturbations such as vacuum pumps and electro-mechanical devices (27 lines, sections 5 and 6), 10 Hz and harmonics (156 lines, sections 5, see also [8]), thermally excited modes of the mirror mass (8 lines, section 7), violin modes of mirrors' wires (113 lines, section 7) and aliased lines (4 lines, section 8). In the end, 32 lines remain that are not understood.

4. Super attenuator modes and sidebands of calibration lines

Very low frequency lines (up to 3.2 Hz) are from oscillations of the mirrors at the frequency of the mechanical modes of the mirror suspensions (the super attenuator (SA) [1]). The identification of the mode is done using the information contained in [9], where the mechanical transfer function of the north end mirror suspension was compared to its SIESTA simulation [15]. The coherence analysis, described in section 5, revealed that these peaks had a large coherence with vertical seismic signals, meaning that they are mostly excited by vertical ground motion. What happens is that there is a vertical motion of the SA inverted pendulum (IP) stage, which is not actively damped (as the horizontal one is), which then excites, by mechanical coupling, horizontal degrees of freedom at the level of the SA last stage. This effect will be cured soon by the implementation of active vertical damping on all mirror suspensions.

The group of lines between 1109 Hz and 1112 Hz in the PSS list is also related to SA oscillation modes. Figure 1 (top) shows the structure of peaks that are symmetric around the

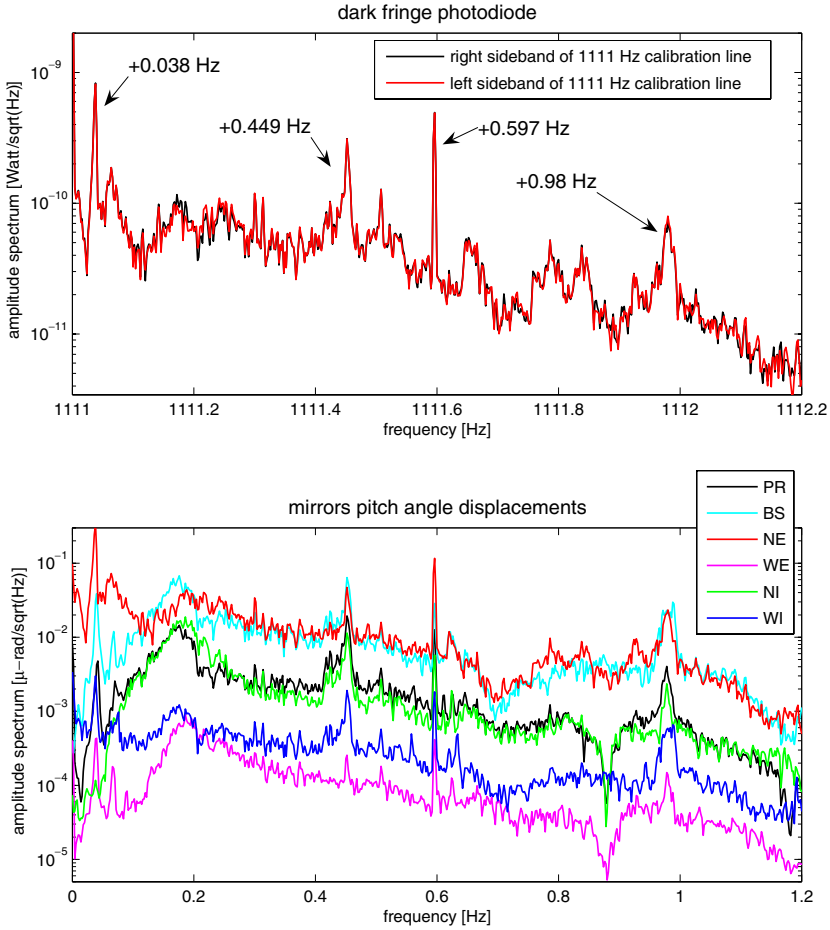

Figure 1. Top: dark fringe photodiode amplitude spectrum showing the sideband structure on the right-side 1111 Hz line. Superimposed (red) is the mirror image of the left-side sideband. Major peaks are at ± 0.038 Hz, ± 0.449 Hz, ± 0.596 Hz, ± 0.981 Hz and ± 3.21 Hz from the 1111 Hz line. Bottom: low-frequency spectral amplitude of alignment error signals measuring the pitch angle of all suspended mirrors. It is apparent that this low-frequency noise is modulating the 1111 Hz line.

1111 Hz line. The 1111 Hz line is a calibration line that modulates the laser frequency. This line gives a measurement of the laser frequency noise. If a mirror tilts then the fringe contrast decreases, and consequently the common mode noise coupling increases. This is a source of non-stationary noise, including the observed burst of bursts (BOBs) [11].

The fact that this structure is symmetric around the 1111 Hz line suggests that it is due to amplitude modulation of the central 1111 Hz line. We noted that values of modulation frequencies (i.e. the distance of peaks from the central line) are typical of super attenuator modes. Another clue as to the source of the noise is the similar structure of the 1111 Hz sidebands and that of the low-frequency component of the mirror alignment signals; this is shown in figure 1.

In order to test the modulation hypothesis, we took a simple sinusoidal signal at 1111 Hz and modulated it with the alignment signals in figure 1 (bottom). A measurable and observable increase in the coherence was found over a 5 Hz band around 1111 Hz between the dark fringe and the modulated signals; the largest coherence is with the signal measuring the pitch angle

of the NE mirror. As a part of the same 'puzzle' we also noted sidebands with a similar structure (and coherence pattern) around other calibration lines, as well as around some other narrow and intense lines. The full understanding was provided by the output plots produced by the *NonStatMoni* monitor [12][15]. It was found that the dark fringe signal is modulated with the residual mirrors angular motion at low frequencies over most of its bandwidth. As a consequence, the low-frequency angular noise couples to every intense spectral line in the dark fringe which is narrow and stationary (such as calibration lines); this increases the spectral noise nearby. This will be cured by increasing the low-frequency gain of alignment control loops, thus reducing the mirrors' slow angular oscillation.

5. Line identification with coherence and multi-coherence tools

A necessary step for the identification of lines originating from electrical or mechanical devices in the laboratory is to search for coherence between the dark fringe and signals from our environmental monitoring instruments: accelerometers, microphones and magnetometers. Such a search was performed (since C6) using a program tool that computes the coherence in 130 s non-overlapping sets of data of the dark fringe photodiode (7.7 mHz resolution) averaged over the entire science mode data segments [3]. The program detects frequency peaks above a cutoff value corresponding to 2.5 standard deviations above the mean coherence in the frequency band of interest[16].

A multi-coherence analysis is necessary when the dark fringe is coherent with several environmental channels. The multi-coherence allows one to disentangle the contribution of individual noise sources. This tool is present in the Virgo NAP library [4]; it accounts for correlations among channels, and gives as output the disentangled noise contributions and the reference signal with the noise removed. We performed a multi-coherence analysis of the magnetic noise in the C7 dark fringe signal. Several noise lines and structures have been detected, among which is an intense 10 Hz line and its higher order harmonics. The analysis indicates a strong coherence with magnetic channels in the central building, suggesting a source located there. The origin of the 10 Hz noise source was then identified as electromagnetic noise emitted from the digitization boards for some digital cameras (see details in section 6). For a thorough analysis of the 10 Hz noise in the PSS analysis of C7 data, see [8].

6. Experimental search of line sources

The list of frequency peaks from the environmental coherence catalogue matching with PSS lines gave us clues as to the location and type of the noise source. Using this information, we performed measurements on the magnetic, seismic and acoustic noise emissions by the vacuum pumps, the air conditioners and other major noise sources in the central building, and the north end (NE) and west end (WE) experimental halls. Our portable equipment consisted of one accelerometer (piezo accelerometer model 393B12 by PCB with 0.1 Hz to 4 kHz bandwidth, and sensitivity 10^4 mV g^{-1}), one microphone (CEL-231 by Casella, 10 Hz to 25 kHz bandwidth, dynamic range 3–135 dB SPL, 1 dB accuracy), one magnetic probe (tri-axial Hall effect sensor by Honeywell model HMC2003, spectral sensitivity 40 μ Gauss over 1 kHz

[15] The *NonStatMoni* program monitors the non-stationarity of the dark fringe signal in different frequency bands. This is done by first computing band limited RMS of the data at given time steps (10 s, 100 s, ...), then looking at the spectral composition of the RMS time series and computing coherences.

[16] The 2.5σ threshold was chosen in order to give a reasonable number of coherence lines that could then be investigated in follow-up studies.

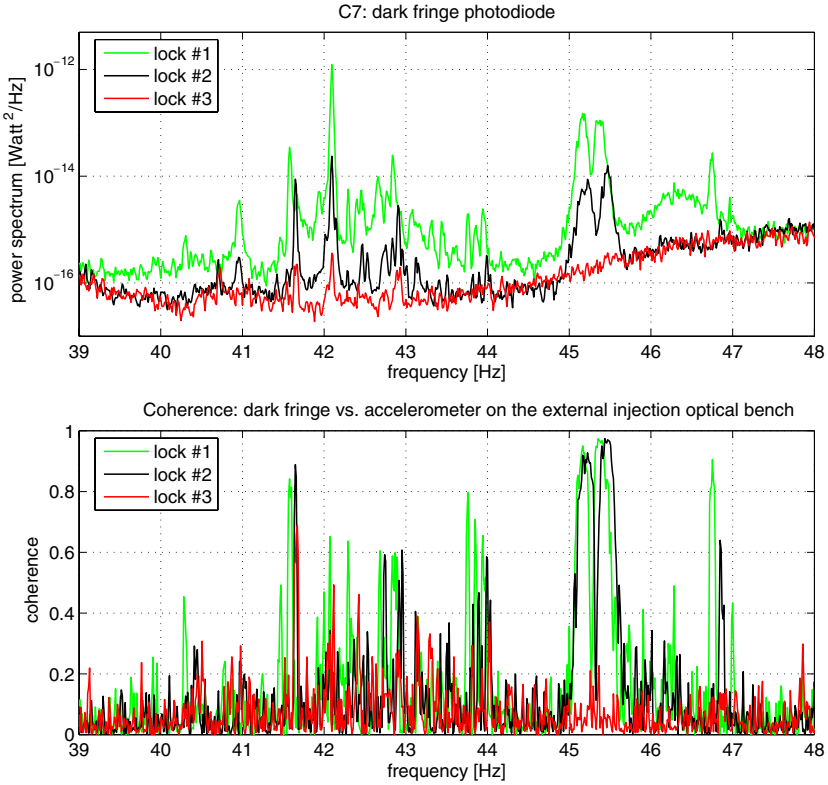

Figure 2. The *horns* at about 45 Hz and nearby noise in C7 dark fringe photodiode at various times during the run: (top) dark fringe photodiode spectrum; (bottom) dark fringe coherence with an accelerometer on the external injection bench. The plots show how the horns disappear when the injection bench vacuum turbo pump is switched off (lock 3). The top plot shows that the amplitude of the nearby noise increases with the detuning of the modulation frequency (backwards from locks 3 to 1). The noise is coherent with seismic noise in and around the laser laboratory.

bandwidth, noise floor 0.13 nT/(Hz)$^{-1/2}$) and one spectrum analyser (Onosokki CF 6400) used for data read out. Below we describe the several measurements performed.

6.1. Turbo pump cooling fans

Two noise 'horns' at about 45 Hz appeared in the C7 dark fringe data (figure 2 (top)) and are particularly intense during the first 25 h of the run. They have a strong coherence with accelerometer sensors inside and around the laser laboratory. On the other hand, the coherence with acoustic sensors is negligible. During the run on the morning of 18 September 2005, as a test, all turbo pumps were switched off in rapid sequence. The horns promptly and completely disappeared from the dark fringe signal in correspondence with the turn off of the injection bench vacuum turbo pump.

Through our measurements in the laboratory we discovered that the sources of this noise were two little cooling fans on the pump enclosure. The small difference in rotation speed of the two fans accounts for the two slightly displaced spectral peaks. For the measurements we placed the portable accelerometer upon the turbo pump vessel. At the same time we measured no magnetic noise, nor any significant acoustic noise produced at these frequencies.

Figure 2 shows another interesting feature, namely that the presence of the horns in the dark fringe signal was reduced in amplitude in correspondence with the (manual) tuning of the laser modulation frequency to match the mode cleaner cavity length. We also observed that there is additional dark fringe noise in the 30–50 Hz frequency region that has similar characteristics as the horns; it is coherent with the same seismic channels and it reduces with the tuning of the laser modulation frequency. Another common feature of this noise and that of the horns is the strong coherence with the angular noise of the mode cleaner cavity optical axis, mainly along the pitch angle degree of freedom. We suspect this additional noise is produced by other mechanical devices inside and around the laser laboratory. One possible explanation for the path by which this noise enters the dark fringe is the following: as described in [10], a mismatch between the modulation frequency and mode cleaner length causes mode cleaner longitudinal noise to couple into the interferometer sensitivity through the error signals used to control the mirrors. Acoustic and seismic noise in the laser laboratory, and vibrations of the external optical bench, produce jitter of the laser beam entering the mode cleaner; this is angular noise that can be converted into longitudinal noise in the presence of an offset of the optical axis.

6.2. Air conditioner

There is a probable coupling of the air conditioner noise to the terminal optical benches. We measured the air conditioning noise with the accelerometer and microphone deployed in different locations inside the NE hall. As a reference, noise lines at 31.7 and 53.2 Hz were used; it was known, from a switch-off test, that these lines originate from the air conditioner. We found that, while acoustic noise is the same everywhere, seismic noise is stronger on the bench and on the top of the bench enclosure than it is on the floor around the bench or at the bench support. Thus, we suspect that the major coupling of the air conditioner noise to the bench is not seismic (i.e through table legs) but acoustic (i.e. air pressure noise shaking optics on the bench). A possible path to the dark fringe is through diffused light, which is reflected back into the interferometer after being scattered by some optical component on the bench.

6.3. Magnetic lines

Searching the central building for strong 10 Hz magnetic emissions with our portable magnetic probe we found the source of the 10 Hz harmonics to be some digitization boards in the data acquisition room. These VME boards receive the analog signal from cameras and digitize them. To do so they send a 10 Hz timing signal to the cameras. The same search revealed the origin of a 10.1 Hz noise line. This line is quite narrow and stationary and quite intense in the central building magnetic sensors. It is generated by the air conditioner of the data acquisition room, as it was eventually demonstrated by its disappearance in correspondence to the machine switch off.

7. Mirror and violin modes

At least eight of the resonant modes of the large mirrors have been identified from the lines observed by the PSS; these are the NE, WE, NI and WI butterfly (about 3885 and 3917 Hz) and drum (about 5545 and 5584 Hz) modes. These values were first measured in run C2 [7]. A difference of a few tenths of Hz in the measured mode frequency is due to temperature drifts. The identified line at 7724 Hz resembles a Lorentzian peak. It is a candidate for one of

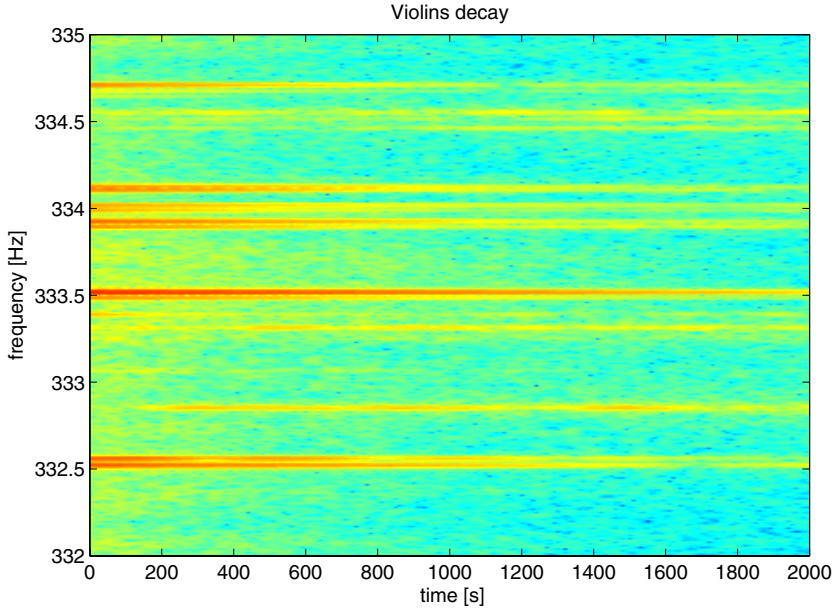

Figure 3. Time frequency map of 2000 s of whitened dark fringe data, starting right after a lock acquisition. This shows the ring down of some violin fundamental modes. The most highly excited ones likely correspond to mirrors that receive correction signals for the lock acquisition.

the higher order mirror modes (mode 0,3) although the finite model simulation in [7] predicts this to be closer to 7600 Hz.

A group of lines in the 330–340 Hz range are the fundamental violin modes of the four wires suspending the NE, WE, NI and WI mirrors, which are thermally excited. These are, in fact, predicted to be at about 320 Hz [13]. In the PSS list, with 100 s time resolution, we identified 28 distinct peaks. There are expected to be 32 distinct fundamental modes. This is because wire tension cannot be perfectly equalized, and $z - x$ degeneracy is removed because the wires are clamped to finite mass bodies with non-diagonal moment of inertia (i.e. $I_{xz} \neq 0$). Higher modes, up to the fourth order, are detected by the line search programs. Higher order modes are not exact multiples of the fundamental ones; each excited wire can be modelled as a coupled oscillator having a non-negligible coupling with the marionette and mirror eigenmodes.

7.1. Ring down of violin and mirror modes

Mirrors and wires are mechanically excited at each lock acquisition and decay to a stationary state within 500–1000 s after the lock is acquired. The transient period is observed by looking at the spectrogram of the whitened dark fringe signal (figure 3). A measurement of the decay time of these modes (i.e. a measurement of Q) is interesting because it provides information on the mirrors' bulk loss angle. The expected Q value for the 3900 Hz mirror (0,2) 'butterfly' mode ranges from 4×10^5 to 1.2×10^6, which corresponds to decay times from 34 to 98 s ($Q = \pi f \tau$) [13, 14].

A rough measurement has been performed using the band limited RMS and lines' amplitude data computed by the *NonStatMoni*. The decay times listed in table 1 are computed

Table 1. Decay time of mirror and wire modes as measured by an exponential fit to the peak frequency amplitude (rows 1 and 2) or the band limited RMS noise (rows 3, 4 and 5) computed by the *NonStatMoni*.

Frequency(Hz)	Description of mode	Decay time(s)
3884	NE and WE mirrors, butterfly mode	106 ± 7
3916	NI and WI mirrors, butterfly mode	510 ± 40
100–200	BS wires, violin modes (peak at 167 Hz)	552 ± 23
300–400	NE, WE, NI and WI wires	520 ± 27
600–700	NE, WE, NI, WI wires (2nd mode)	214 ± 13

by fitting the data with an exponential decay ($Ae^{-t/\tau}$). The estimate has been repeated for several ($N = 13$–20) lock acquisitions and the average values are listed in table 1. Errors are computed as $\sigma/\sqrt{N}$, where σ is the standard deviation of the sample of repeated measurements.

We have also tested a method to fit the decaying signal of one of the modes, the one at 3884.17 Hz, which is associated with the NE mirror mode (0,2) [7]. The mode was first isolated by using an adaptive notch filter centred at this frequency. Then we fit the notched signal to the function

$$y(t) = A_1 e^{-t/\tau_1} \sin(2\pi f_1 t + \phi_1) + A_2 e^{-t/\tau_2} \sin(2\pi f_2 t + \phi_2),$$

where $f_1 = 3884.17$ Hz, and the second term accounts for the residual beating with the same mode of the WE mirror whose frequency is very close ($f_2 = 3884.60$ Hz). The result of the fit is $\tau_1 = (118.5 \pm 0.6)$ s.

The frequencies of these wire and mirror modes are in the audible band, and the frequency of the first violin modes is close to a 'Mi' tone (329.63 Hz). We have isolated some of these wires and mirror sounds by applying a narrow band pass filter. These have been used, together with other 'Virgo sounds', in a musical performance, namely part of the celebrations of the 500 years since Galileo Galilei[17].

8. Aliased lines

We realized that a few of the lines in the PSS list are the result of the aliasing of higher frequency lines. The PSS program used the h_4 kHz channel, which is the h-reconstructed channel down-sampled from 20 kHz to 4 kHz. The down-sampling procedure applies anti-aliasing filtering to the data using one sixth-order Butterworth filter with a cut off at 2 kHz. It has been noted that more efficient anti-aliasing filters must be used with future data.

9. Conclusions

We have described the analysis of spectral lines in the dark fringe photodiode signal of the C7 run. We adopted, as a new line catalogue, the frequency peak list produced by the analysis pipeline of the periodic signal search. This catalogue compares well with the output of our line search algorithm. The newly implemented environmental coherence catalogue and the multi-coherence applied to environmental channels proved to be very useful tools in identifying lines of environmental origin, and also providing an aid in the location of these noise sources. Eventually, experimental hunts allowed us to precisely locate the source of several lines. It has been possible to identify the source of most of the lines detected by the search algorithms.

[17] Pisa, June 2006, http://www.fabbricaeuropa.com.

This information has been stored in an on-line database [16] and is being used to understand the interferometer noise, both during commissioning or with gravitational wave searches. For example, the PSS analysis of the subsequent Virgo weekend science runs (WSR) data used the list of identified lines to veto these frequencies from the peak maps; about 1% of the PSS pulsar candidates were vetoed in the WSR7 science run by using the lines that we have identified in our analysis of the C7 data.

References

[1] Acernese F *et al* 2007 The status of Virgo detector *Class. Quantum. Grav.* **24** S381
[2] Chassande-Mottin E and Fiori I 2004 *Class. Quantum Grav.* **22** S1189
[3] The Virgo environmental coherence catalog for C7 run
http://wwwcascina. virgo. infn. it/DataAnalysis/Noise/doc/C7/coherence/webpage/catalogue. html
[4] Cuoco E 2004 *Class. Quantum Grav.* **22** S1041
[5] Acernese F *et al* 2007 Coincidence analysis between periodic source candidates in C6 and C7 Virgo data *Class. Quantum Grav.* **24** S491
[6] Fiori I, Paoletti F, Pasqualetti A and Soldani D 2003 Noise and spectral lines from motor devices *Virgo note* VIR-NOT-PIS-1390-253
[7] Puppo P 2004 A finite element model of the Virgo mirrors *Virgo note* VIR-NOT-ROM-1390-262
[8] Frasca S http://grwavsf.roma1.infn.it/pss/reports/10Hzdeltas.pdf
[9] Fiori I, Braccini S, Travasso F and Vicerè A 2004 Siesta simulation of NE suspension tower *Virgo note* VIR-NOT-PIS-1390-285
[10] Flaminio R, Gouaty R and Tournefier E 2006 Analysis of the sensitivity of the recycled interferometer during C5, C6 and C7 runs *Virgo note* VIR-NOT-LAP-1390-313
[11] Bizouard M A, Cavalier F, Christensen N and Hello P 2007 Data quality and Veto studies for the GW bursts search in C7 run data *Virgo note* VIRGO-NOT-LAL-139-337
[12] The Virgo monitor of non-stationarieties http://wwwcascina. virgo. infn. it/MonitoringWeb/NonStatMoni/
[13] Punturo M 2004 The Virgo sensitivity curve *Virgo note* VIR-NOT-PER-1390-51
[14] Punturo M and Travasso F 2004 Evaluation of the bulk loss angle of the Virgo mirrors from C2 data *Virgo note* VIR-NOT-PER-1390-263
[15] Caron B *et al* 1999 SIESTA, a time domain, general purpose simulation program for the VIRGO experiment *Astropart. Phys.* **10** 369–86
[16] The Virgo line database https://pub3. ego-gw. it/linesdb/